Advanced Composite Materials
Publication details, including instructions for authors and subscription information:
http://www.tandfonline.com/loi/tacm20

Carbon-carbon composite turbine disk for the air turbo ramjet engine (ATREX)

Ken Goto , Hiroshi Hatta , Yasuo Kogo , Hiroshi Fukuda , Tetsuya Sato & Nobuhiro Tanatsugu

Version of record first published: 02 Apr 2012.

To cite this article: Ken Goto , Hiroshi Hatta , Yasuo Kogo , Hiroshi Fukuda , Tetsuya Sato & Nobuhiro Tanatsugu (2003): Carbon-carbon composite turbine disk for the air turbo ramjet engine (ATREX) , Advanced Composite Materials, 12:2-3, 205-222

To link to this article: http://dx.doi.org/10.1163/156855103772658560

Adv. Composite Mater., Vol. 12, No. 2-3, pp. 205–222 (2003)

Also available online - www.vsppub.com

Carbon-carbon composite turbine disk for the air turbo ramjet engine (ATREX)

KEN GOTO [1], HIROSHI HATTA [1,*], YASUO KOGO [2], HIROSHI FUKUDA [2], TETSUYA SATO [1] and NOBUHIRO TANATSUGU [1]

[1] *Division for Space Propulsion, The Institute of Space and Astronautical Science, 3-1-1 Yoshinodai, Sagamihara, Kanagawa, 229-8510, Japan*

[2] *Department of Material Science and Technology, Faculty of Industrial Science and Technology, Tokyo University of Science, 2641, Yamazaki, Noda, Chiba, 278-8510, Japan*

Received 4 July 2002; accepted 28 October 2002

Abstract—A feasibility study of three-dimensionally fiber-reinforced carbon-carbon composites (3D-C/Cs) for application to a turbine disk of ATREX (Air turbo ramjet engine with expander cycle) was carried out. Spin burst tests at room temperature were conducted using 3D-C/C disks, and the fracture behaviors were characterized. A 3D-C/C disk was totally fractured at a peripheral speed of 516 m/s ($r = 150$ mm), which is sufficient for the ATREX application. However, fiber bundles at the disk periphery prematurely suffered micro-scale damage, and fragments of the fiber bundle unit flew out before total fracture occurred. In order to prevent the fly-out behavior, the disk was impregnated with Si only near its periphery. Although this treatment increased the initiation speed of the fly-out behavior, this improvement was considered insufficient for purposes of the ATREX application. Next, a simplified analysis was conducted to characterize the fly-out behavior. Based on this analysis, the following three measures were discussed: (1) decreasing bundle thickness (i.e. using fine fiber texture), (2) increasing toughness of the fiber bundle interface, and (3) minimizing local curvature in waviness of the fiber bundles in the circumferential direction.

Keywords: Carbon/carbon composite; turbine disk; spin burst; air turbo ramjet.

1. INTRODUCTION

A two-stages-to-orbit (TSTO) type space plane for a future space transportation has been studied in the Institute of Space and Astronautical Science, Japan. In this study, an air turbo ramjet engine was chosen as the most suitable candidate for the first

*To whom correspondence should be addressed. E-mail: hatta@pub.isas.ac.jp

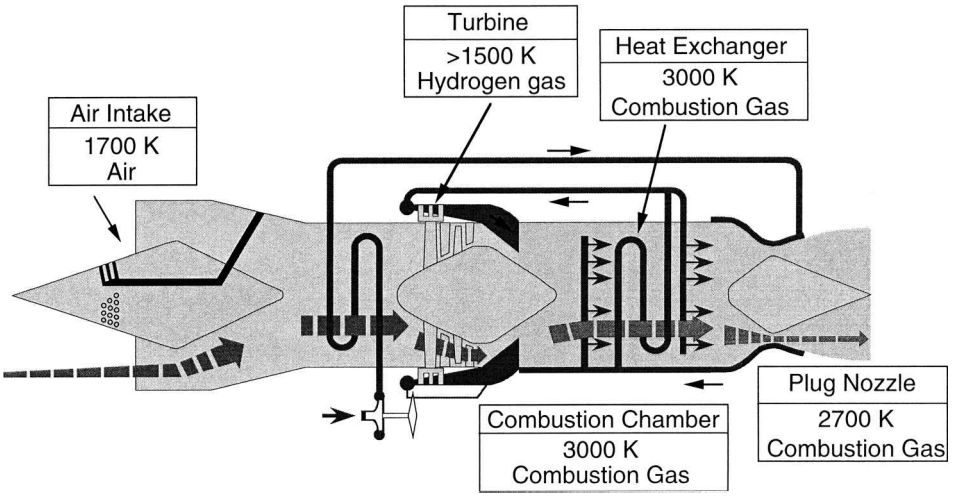

Figure 1. Flow diagram and high temperature structures of ATREX. The atmosphere and the maximum temperature are also shown.

stage propulsion system of a perfectly recycled TSTO space plane [1, 2]. The air turbo ramjet engine with expander cycle (ATREX) is expected to possess effective thrust up to mach 6 at an altitude of 35 km. As shown in Fig. 1, the ATREX is designed to use liquid hydrogen to cool intake air to the fan, and fuel gas (H_2) is reheated up by combustion gas to drive the turbo-machinery. A high level of heat resistance is required for the various engine components for the ATREX [1, 2].

Carbon-carbon composites (C/Cs) can maintain high strength and toughness up to temperatures higher than 2273 K and simultaneously possess low density less than 2000 kg/m^3. Based on these strong advantages, C/Cs have been expected to be used for the turbine disk of the ATREX. The preliminary requirements of the turbine disk for the ATREX are as follows: (1) disk diameter equal to 400 mm, (2) peripheral speed at the disk tip faster than 390 m/s, (3) high temperature atmosphere of hydrogen gas (>1500 K). Because of its axi-symmetric shape, an r-θ-z three-dimensionally fiber-reinforced C/C (3D-C/C) is considered to be a promising candidate [3] for the turbine disk.

Over the last two decades, feasibility studies of a C/C turbine disk have been carried out [4–8]; however, none of them led to actual use. Central to these failures was the rapid strength degradation caused by oxidation; the final goal of these projects was to develop a turbine disk powered by an exhaust gas containing oxygen. To that end, industries are now attempting to use, for example, continuous fiber-reinforced SiC matrix composites [6, 9], though the strengths and maximum operation temperatures of SiC-based composites are lower than those of C/Cs. In fact, oxidation is not problematic in the ATREX, because the operational gas is heated hydrogen, and the period of exposure to severe temperature is less than 5 minutes per flight [1–3].

Fracture behavior of disks comprised of brittle materials (e.g. polycrystalline graphite or cast iron) has depended on the disk geometry, i.e. the ratio between the inner and outer radii, r_i/r_o [10, 11]. When $r_i/r_o \geqslant 0.5$, fracture occurred when the average stress in the hoop direction, $\bar{\sigma}_\theta$, reached the tensile strength of the material (average hoop stress criterion). However, the fracture speed of the disk was degraded by the effect of stress concentration at the inner radius when $r_i/r_o < 0.5$. In contrast, the fracture of CFRP (carbon-fiber-reinforced plastic) has been reported to follow Hoffman's law or maximum stress criterion [12–14]. Recently, Kogo *et al*. studied the fracture behavior of a laminated C/C (2D-C/C) disk [15], and showed that fracture occurred following the average hoop stress criterion even at $r_i/r_o = 0.2$. In the rotation tests of 3D-C/C disks, micro-fractures are usually observed before the total fracture [4, 5]. Ogawa *et al*. reported that small fragments flew out from the surface of a 3D C/C disk during a rotation test, and the rotational fracture test was abandoned due to extensive growth of disk vibration caused by the flown-out fragments [8]. This fly-out behavior has not yet been analyzed, and no effective preventive technique has been established.

In the present study, the spin fracture behavior of 3D-C/C disks was studied to examine the applicability of such composites for the turbine disk of the ATREX. Emphasis here was placed on explanation of the fly-out behavior. A semi-quantitative model was constructed based on the experimental evidences. Then, based on the model, attempts were made to prevent the fly-out phenomenon. Finally, the fly-out behavior from the tail ends of turbine blades was also examined.

2. EXPERIMENTAL PROCEDURE

2.1. Materials

Two types of r-θ-z 3D-C/C disks, Disks A and B, were rotation-tested. Disk-As were fabricated to be 200 mm in diameter and 10 mm in thickness by Arisawa Seisakusyo Co. Ltd. These disks were reinforced with a high modulus type carbon fiber (TORAYCA®, M46J, Toray Co. Ltd.), and the fiber volume fractions in r, θ, and z directions were $f_r = 10\%$, $f_\theta = 40\%$, and $f_z = 5\%$, respectively. Disk-Bs, 400 mm in diameter with a thickness of 10 mm, were fabricated by Aerospatiale Corp. (now EADS, France). In these disks, a high strength type carbon fiber (TORAYCA®, T-800, Toray Co. Ltd.) was used. The fiber volume fractions were set to $f_r = 5\%$, $f_\theta = 40\%$, $f_z = 10\%$.

The 3D-C/Cs were produced by infiltrating matrix precursor into three-dimensional fabrics by liquid processing routes. Coal-tar pitch was used as the precursor for Disk A and phenolic resin for Disk B. The densification of Disk A was conducted by Nippon Carbon Corp., and that of Disk B by Aerospatiale Corp. The infiltrated precursor was converted to carbon at 1273 K (carbonization), and finally heat-treated at 2273 K (graphitization). The process cycle (infiltration, carbonization and graphitization) was repeated several times. The bulk density finally reached

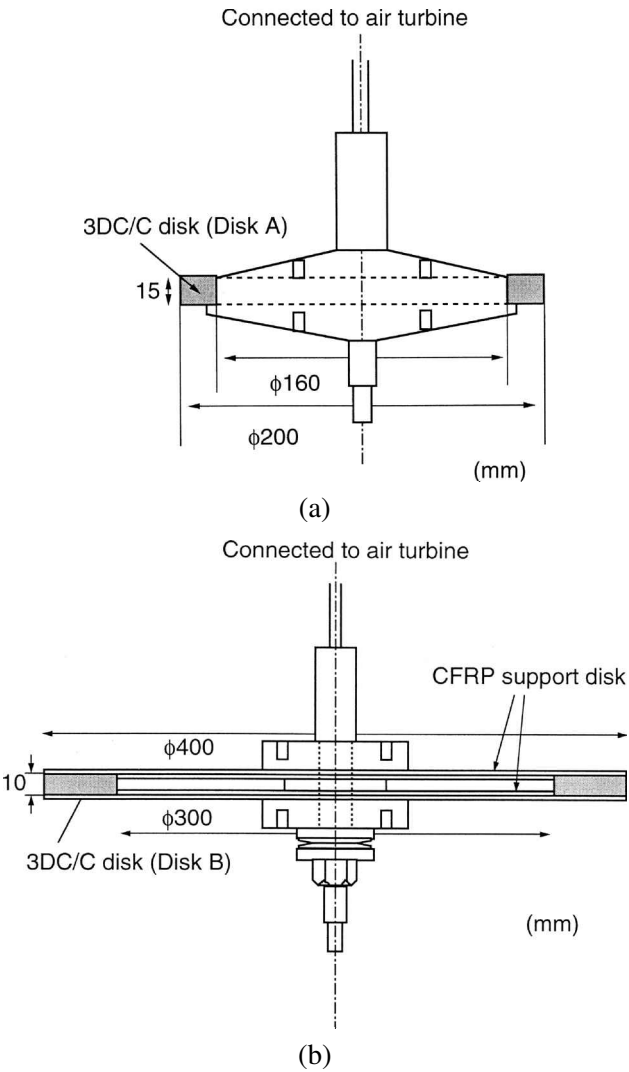

Figure 2. Shape and dimensions of the specimens and rotation fixtures for (a) Disk A, (b) Disk B, and (c) simulated turbine blades. Fiber orientation of the simulation blade is also shown.

was 1640 kg/m^3 for Disk A and 1420 kg/m^3 for Disk B. The fabricated 3D-C/Cs were machined into their final shapes by a milling technique, as shown in Fig. 2a and b.

Specimens used for the simulation of turbine blades are shown in Fig. 2c. The simulated blades were machined by conventional milling technique from an orthogonally reinforced 3D-C/C plate impregnated by a liquid route using pitch supplied by Toho Tenax Corp. (Tokyo, Japan). In order to examine the shapeability of the blade tail-edge, the tip radius of the simulated blades was varied from 0.1 to 1.0 mm. The fiber for this 3D-C/C plate was of a high strength type

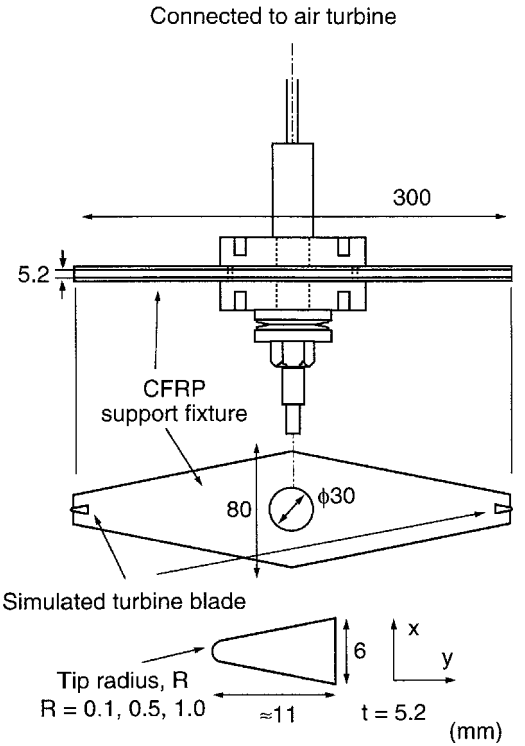

(c)

Figure 2. (Continued).

(Besfite® IM-600, Toho Tenax Corp.), and the volume fractions of the fiber were $f_x = 40\%$, $f_y = 15\%$, and $f_z = 3\%$. This plate was finally heat-treated at 2573 K to attain a bulk density of 1800 kg/m^3. The orientation of the fiber in the simulated blades was set to match with that in blades machined from the 3DC/C disks, as shown in Fig. 2c.

The fly-out behavior was believed to be caused by poor adhesion between fiber bundles. As a preventive technique against the fly-out behavior, partial silicon impregnation was performed on Disk B, aiming at enhancement of bonding between fiber bundles. Two different silicon impregnation processes were performed, one by liquid Si infiltration (Nihon Gaishi Co. Ltd.) and the other by a chemical vapor infiltration technique (Toshiba Ceramics Corp.).

2.2. Mechanical test

Cold spin tests were carried out in a vacuum chamber using a spin tester driven by an air turbine (maximum test weight = 10 kg, Maruwa electric Corp.). Disk A was mounted directly on a steel rotor (Fig. 2a) and Disk B was mounted on CFRP fixtures (Fig. 2b). The simulated turbine blades were mounted on the spin tester using a specially designed CFRP fixture, as shown in Fig. 2c. An assembled rotor

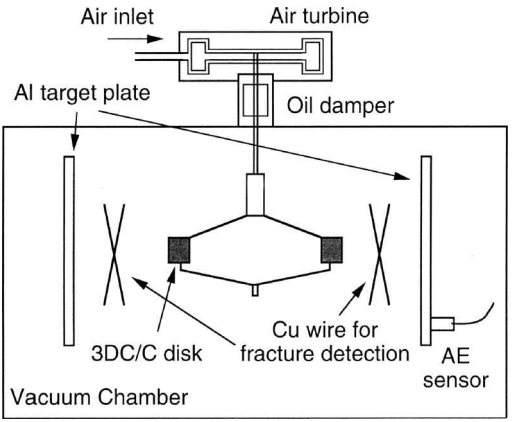

Figure 3. Schematic drawing of spin tester setup.

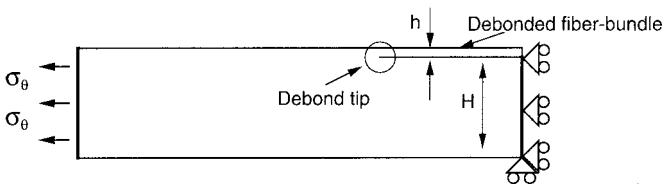

Figure 4. Loading and constraint conditions for FEA.

Table 1.
Elastic moduli of Disk B assumed in analysis

E_r*	E_θ*	E_z*	$G_{r\theta}$*	$G_{\theta z}$*	G_{rz}*	$\nu_{r\theta}$	ν_{rz}	$\nu_{\theta z}$
19	156	39	7.0	7.0	5.1	0.05	0.3	0.09

* (GPa).

was adjusted to achieve rotation balance using a rotation balance tester (FH216, Akashi Co. Ltd.). The rotation tests were conducted at room temperature with a constant acceleration speed of 100 rpm/s under reduced pressure of less than 10 Pa. A fine copper wire was set around a specimen to detect large scale fracture by cutting the wire with fractured fragments. Small fragments flying out from a C/C were detected by an AE sensor (AE-901, NF Electric Corp.) adhered to an aluminum plate target 1-mm thick and located around the specimen. Figure 3 schematically shows the spin tester with a specimen and the detection systems.

2.3. Finite element analysis

To understand the fly-out behavior, finite element analysis (FEA) of a debonded fiber bundle located along the peripheral surface of a disk was conducted. Figure 4 shows the loading and constraint conditions used in the FEA. This model was composed of 8-node quadratic elements. Stress analysis was conducted under the

plane strain condition using ABAQUS version 5.7. The size of the mesh around the debonded layer was reduced until the computed results showed a negligible difference. The energy release rate at the tip of a debonded fiber-bundle was estimated by this analysis. The anisotoropic elastic response was assumed in the FEA with the elastic moduli as listed in Table 1, where E, G, and ν represent Young's modulus, shear modulus, and Poisson's ratio, and subscripts r, θ, and z represent the directions, respectively.

3. RESULTS AND DISCUSSION

3.1. Fracture behavior of Disk A

Figure 5 shows the fracture appearance of Disk A. This disk was finally fractured into 6 segments at a peripheral speed at the outer radius ($r_o = 100$ mm) of 516 m/s, and this speed satisfied the requirement for the ATREX turbine disk. Disk A had an inner/outer ratio, r_i/r_o, of 0.8, and the hoop stress, σ_θ, of the rotating disk gradually decreased from r_i to r_o. The deviation of σ_θ from the average was within $\pm 15\%$. The average σ_θ at the fracture was estimated to be about 360 MPa, and the average hoop strain to failure was about 0.22%, under the assumption that the stress–strain curve was linear [16, 17]. The maximum hoop stress appearing at r_i was 420 MPa. On the other hand, the tensile fracture stress of Disk A material was 370 ± 30 MPa. This strength was obtained using an orthogonally reinforced

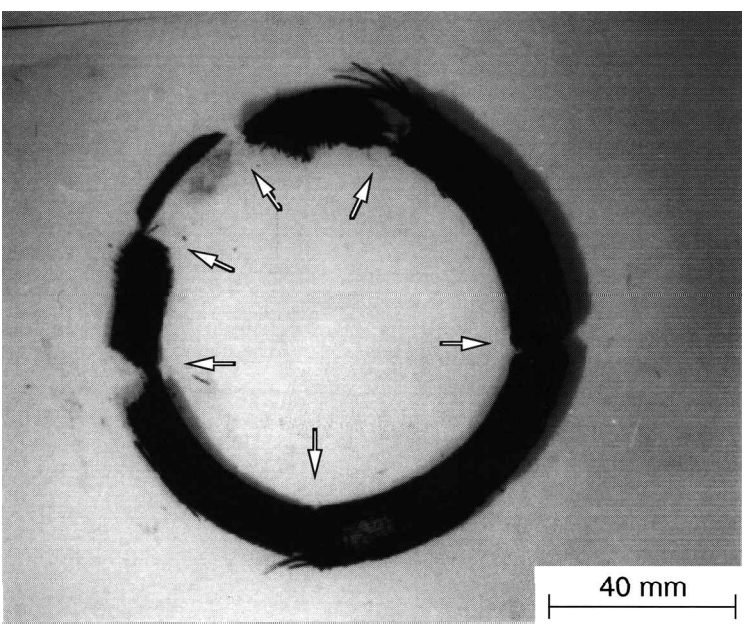

Figure 5. Fracture appearance of Disk A after total fracture at peripheral speed of 516 m/s at outer radius. Arrows indicate the boundaries of the fractured sections.

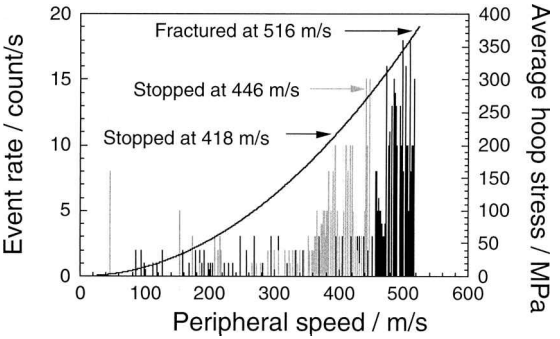

Figure 6. AE event rate as a function of rotation speed. Average hoop stresses of Disk A are also shown.

3D-C/C plate with the same carbon fiber, fiber architecture, and the same process route as those of the disk [18]. Consequently, it was concluded that Disk A was fractured under the average stress criterion [15].

Figure 6 shows the AE event rate and the average hoop stress as a function of the peripheral speed of the disk. As illustrated in this figure, the rotation tests were interrupted at speeds of 418 m/s and 446 m/s due to abrupt increase in the AE event rate; dotted and solid bars represent AE event rates for the runs up to 446 and 516 m/s, respectively. At each run, the fiber bundles were observed to fly-out from the surface of the disk. It should be noted in Fig. 6 that the AE event rate abruptly increased from the maximum speed of the previous run. This result indicates that there were unstable specific locations in the disk where the fly-out phenomenon easily occurred. Simultaneous with the fiber bundle fly-out, shaft vibration slightly increased because of the increase in rotational imbalance. The small number of AE events before the abrupt increase were confirmed to be small carbon particles ejected from the matrix pockets.

3.2. Fracture behavior of Disk B

Disk Bs were fabricated to confirm the feasibility of 3D-C/C at real size. However, these disks contained strong local waviness, as shown in Fig. 7. Thus, the fly-out of fiber bundles was detected at the speed of ≈250 m/s (r_o = 200 mm), which was much lower than that for Disk As. The tensile strength of Disk B in the circumferential direction was estimated to be at least 310 MPa under the assumption that the fracture occurred at the average fracture strain in the hoop direction was 0.2%. The average hoop stress ($\bar{\sigma}_\theta$) at 250 m/s was only 30% of the expected minimum strength. Figure 8 shows the peripheral surface of the 3DC/C disk (Disk B) after rotation test at the maximum speed of 270 m/s. In this figure, fiber bundles oriented in the radial direction apparently protrude. This indicates that fiber-bundles placed in the θ and z directions were flown-out from the disk. As was observed in the case of Disk As, shaft vibration simultaneously increased after the onset of fly-out behavior. Nevertheless, rotation test was again attempted after

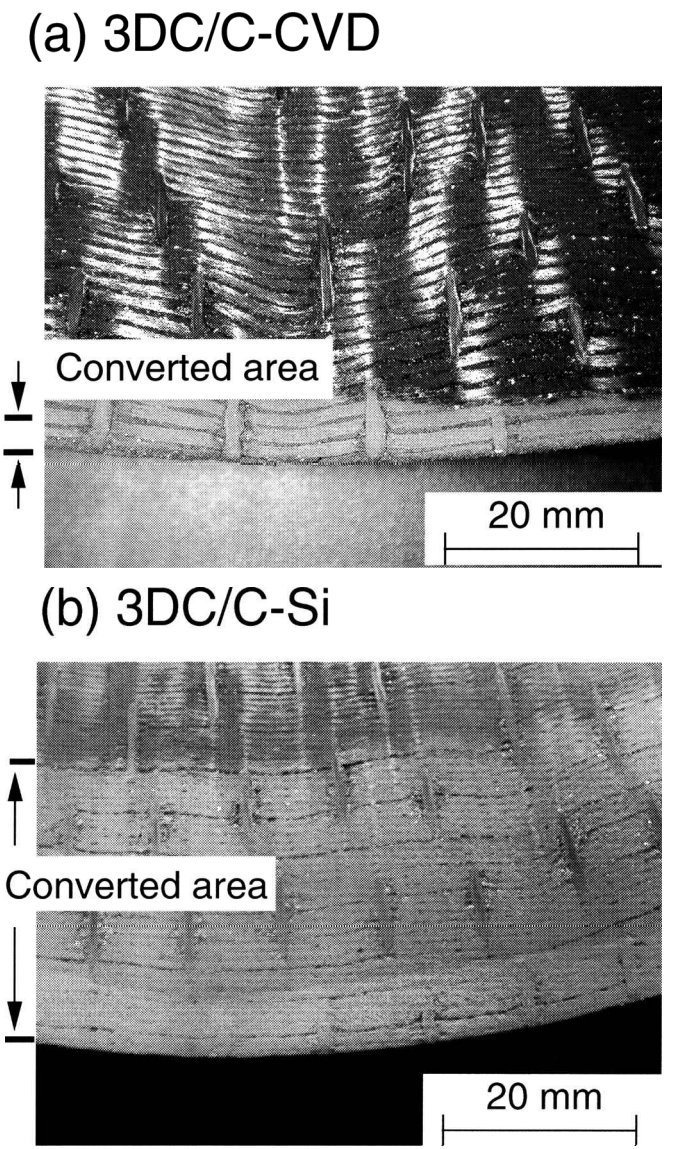

Figure 7. Surface of Disk B after the onset of fly-out behavior at peripheral speed of 270 m/s at outer edge.

adjustment of rotation balance. However, the rotation test was finally aborted at 320 m/s because the shaft vibration became too large.

3.3. Fly-out behavior

Fly-out of the unit of fiber bundles from the peripheral surface of the 3D-C/C disks occurred. Hence, debonding between fiber bundles is assumed to be precede the fly-out. Observation of the disk after the fly-out was initiated revealed that debonding

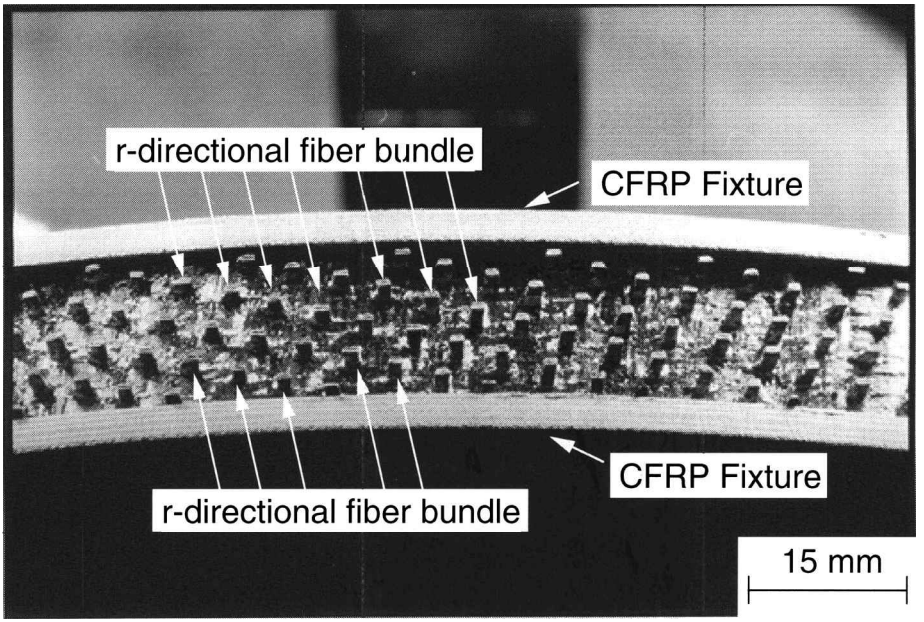

Figure 8. Disk B with partial Si conversion by (a) the gaseous route and by (b) liquid Si impregnation.

of fiber bundles occurred at places in which a fiber bundle oriented in the θ direction (θ-bundle) was heavily waved and sharply terminated by machining, as shown in Fig. 9a. If the θ-bundles were wound without waviness, like those shown in Fig. 9b, no cut fibers should appear on the outer peripheral surface. Thus, it can be concluded that such local curvature of the textile causes debonding of the fiber bundles and fly-out behavior. The local curvature of the fiber bundles in Disk B was likely caused by inserting the r- and z-bundles during the 3D-preform fabrication process and by shrinkage during carbonization of impregnated resin [4, 5].

3.4. Modeling of fly-out phenomenon

Based on the above observations, the fly-out behavior was modeled as shown in Fig. 10. In this model, θ-bundles on the peripheral surface first assumed to be first debonded at the bundle end primarily due to the hoop stress in the disk (Fig. 10a). The bundle ends were actually formed by the machining of waved fiber bundles. Next, this debonding is assumed to extend (Fig. 10b), and, finally, long debonded fiber-bundle fracture occurs by bending caused by the centrifugal force (Fig. 10c). At the interface of the fiber bundles, two types of force exert influence: hoop stress generated in the disk and centrifugal force directly loaded to the debonded fiber bundle, as shown in Fig 11. Considering these two loading modes, the total energy release rate at the debonding tip, G^{total}, can be expressed as $G^{\text{total}} = G^{\text{deb}} + G^{\text{cent}}$, where G^{deb} and G^{cent} are energy release rates induced by the hoop stress and the centrifugal force, respectively. Hutchinson and Suo [21] made a numerical analysis

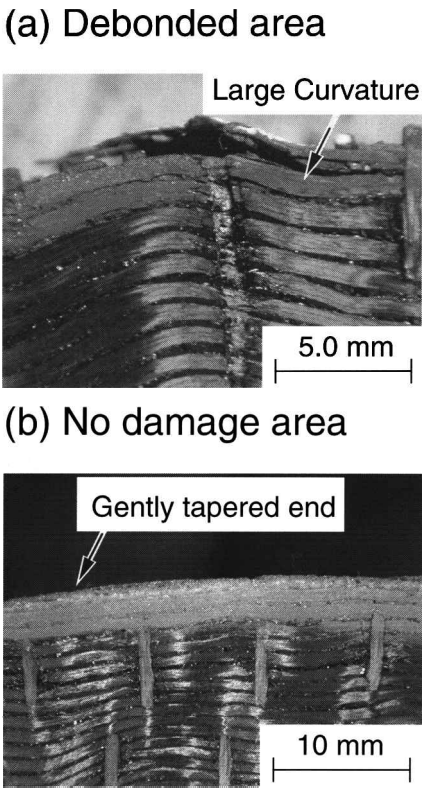

Figure 9. Surface of Disk B with partial Si conversion by (a) the gaseous route and by (b) liquid Si impregnation.

on the tip of a debonded layer under a similar loading condition with G^{deb} for isotropic material. According to their analysis, G^{deb} decreases with increasing debonding length and finally saturates. The saturated G^{deb} was given by

$$G^{\mathrm{deb}} = \frac{\bar{\sigma}_\theta^2 h A}{2E_\theta}, \tag{1}$$

$$A = 1 + 4\frac{h}{H} + 6\left(\frac{h}{H}\right)^2 + 3\left(\frac{h}{H}\right)^3, \tag{2}$$

where $\bar{\sigma}_\theta$ is the average hoop stress, ρ is bulk density, ω is angular velocity, and h and H are the thickness of the debonded layer and the remaining substrate, respectively. Equation (1) is effective only when the debonded length, a, becomes larger than 10-times h. G^{cent} can be estimated by modifying the shape function of a cantilever beam specimen [22] as follows:

$$G^{\mathrm{cent}} = \frac{3r_{\mathrm{o}}^2\rho^2\omega^4 a^4}{2h(1-\nu_{\theta r}^2)}\left(\frac{1}{2E_\theta E_r}\right)^{1/2}\left[\left(\frac{E_\theta}{E_r}\right)^{1/2} + \frac{E_\theta}{2}\left(\frac{-2\nu_{r\theta}}{E_\theta} + \frac{1}{G_{r\theta}}\right)\right]^{1/2}. \tag{3}$$

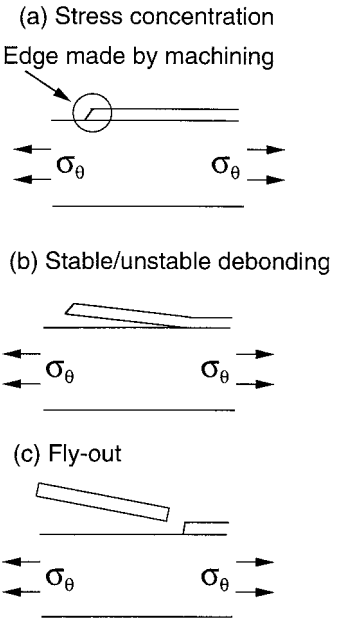

Figure 10. Termination of the fiber bundles after spin test at the sharply machined end (a) and the gently machined end (b). Fiber-bundle debonding initiated at the sharply terminated end and appearing at the surface originates from large curvature of the fiber bundles.

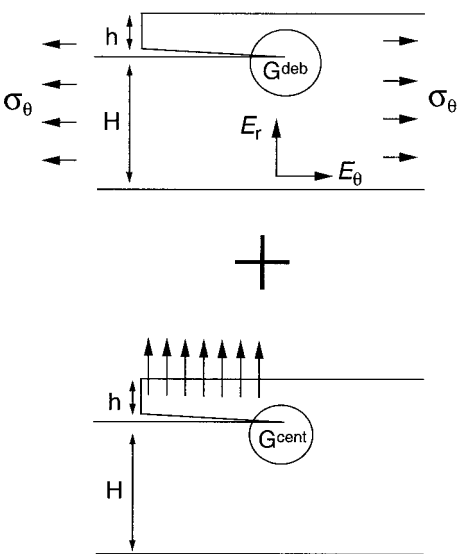

Figure 11. Fracture model for fly-out behavior, the initiation of the fiber-bundle debonding (a), unstable debonding (b), and failure of fiber bundle to fly-out (c).

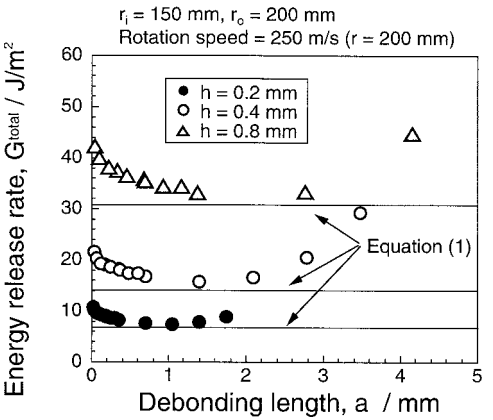

Figure 12. Loading modes for debonded fiber bundle for first order approximation.

To obtain accurate G^{total}, FEA was also performed as functions of a and h, and the calculation results are shown in Fig. 12. As can be seen in Fig. 12, G^{total} shows the minimum. The onset of fly-out can be described by the condition that the minimum G^{total} equals the critical energy release rate of the inter-bundle, G_c. The minimum G^{total} is near to the value from equation (1), as shown by the horizontal lines in Fig. 12. The minimum G^{total} of the 3DC/C disk used in this study was estimated to be $\approx$33 J/m^2 (h = 0.8 mm), and this value was comparable to G_c for various polycrystalline graphites (10 to 150 J/m^2) [23].

As shown in Fig. 12, G^{total} depends on the bundle thickness, h; G^{total} degrades with the decrease of h. This means that a C/C disk with a finer texture (smaller h) can sustain a higher rotation speed. To illustrate the effect of h, the critical speed for fly-out behavior was shown as a function of h for various G_c in Fig. 13. This figure indicates that G_c must be enhanced to 200 J/m^2 to satisfy the operation condition of the ATREX using fiber architecture identical to that of Disk B. If a disk possesses G_c identical to that of Disk B, h must be less than 0.2 mm, and if G_c can be improved to the level of polycrystalline graphite, 100 J/m^2 [23], the fiber-bundle thickness must be smaller than 0.5 mm.

3.5. Suppression of fly-out phenomenon

Based on the above discussions, three measures to improve the fly-out rotation speed are considered:

(i) decreasing bundle thickness (i.e. using finer fiber texture),

(ii) reducing local curvature in the circumferential fiber bundle, and

(iii) increasing G_c or improving bonding strength between the fiber bundles.

Disk Bs used θ-bundles with 36 000 filaments, and Disk As θ-bundles with 12 000 filaments. The thickness h of Disks A and B were 0.45 mm and 0.8 mm, and the fly-out initiated for Disks A and B was 370 m/s and 250 m/s, respectively. Thus, from

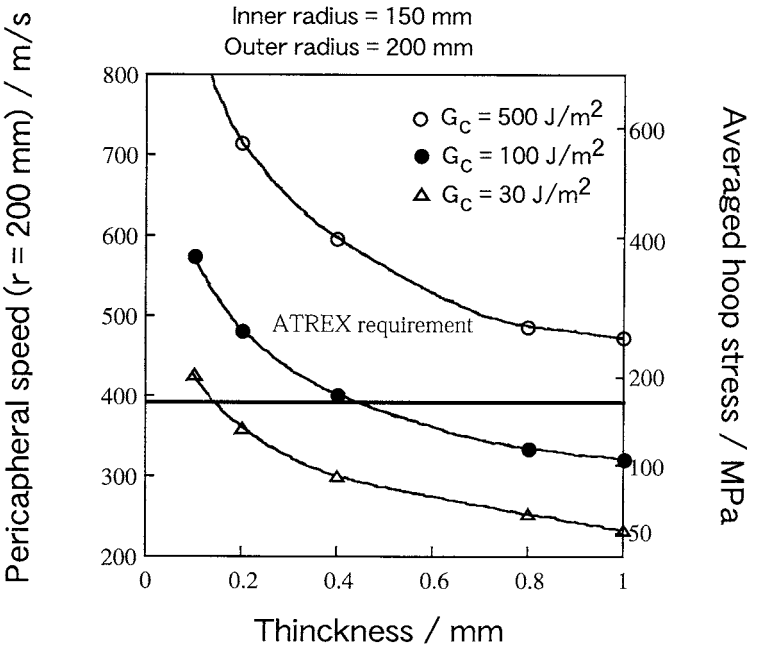

Figure 13. Total energy release rate, G^{total}, at the debonding tip versus debonded length as a function of the thickness of fiber bundles at the onset of fly-out behavior for Disk B. The results from equation (1) are also shown.

Fig. 13, the reduction of the fly-out speed in Disk B can be understood in terms of the effect of h. The minimum size of commercially available fiber bundles is 1000 filaments. If this fiber bundle can be used, h will be reduced to 0.13 mm. In view of Fig. 13, this value of h is sufficient. However, it is rather difficult to use fine fiber bundles in large-size 3D-preforms. Thus, an alternative approach must be explored.

The largest improvement is expected if effective measures are taken to reduce the local curvature. For reduction of local curvature, the weaving process of the preform is most important. The other source of local curvature in 3D-preform is shrinkage of the matrix precursor in the carbonization process. The deformation of the 3D-preform during carbonization can be minimized by using appropriate jigs. However, it is difficult to evaluate both effects quantitatively.

For bonding strength enhancement of the inter-fiber bundles, impregnation of more carbon matrices or carbides might be effective. In the present study, an attempt was made to impregnate C/Cs with molten Si into for the enhancement of inter-bundle bonding strength [19, 20]. To examine the actual effect of this, molten Si was impregnated only near the peripheral surface of Disk B. Figure 7a and b, shows Disk B treated with partial Si impregnation by (a) the gaseous route (3DC/C-CVD) and (b) by liquid Si impregnation (3DC/C-Si), respectively. As shown in these photographs, 3DC/C-CVD was converted into SiC at a thickness of 10 mm and 3DC/C-Si at a thickness of 40 mm from the peripheral surface.

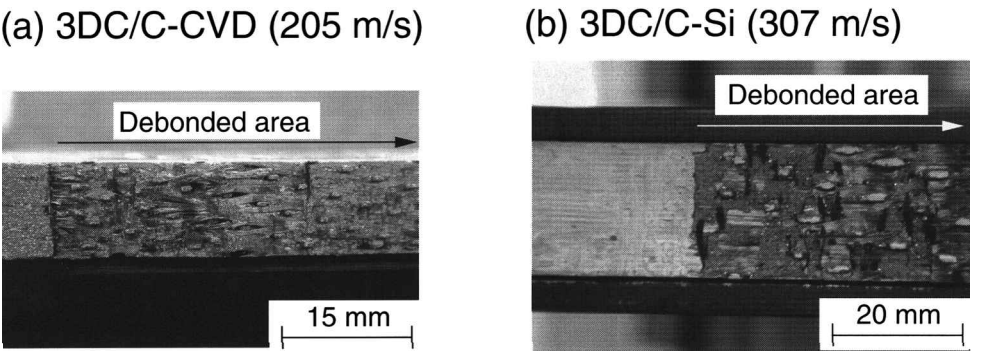

Figure 14. Fracture mode mapping of 3DC/C disk. Fly-out behavior or disk fracture as a function of fiber-bundle thickness and critical energy release rate between fiber bundles.

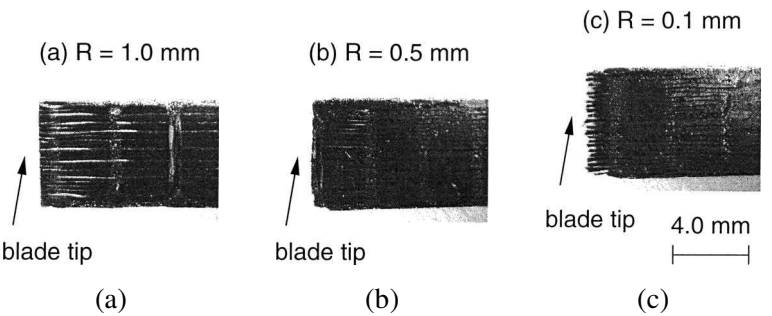

Figure 15. Edges of simulated turbine blades machined from 3DC/C by conventional milling technique with changing tip radii, R, of (a) $R = 1.0$ mm, (b) $R = 0.5$ mm, and (c) $R = 0.1$ mm.

An ideal impregnation is only 3 or 4 bundles from the surface so as to avoid serious degradation of tensile strength. The cold spin tests of these disks resulted in the onset speeds for fly-out behavior of 188 m/s for 3DC/C-CVD and 307 m/s for 3DC/C-Si. The fragments flown-out from both disks were Si-converted fiber bundles. The observation of the surfaces after fly-out behavior revealed that most of the debonded surface of the 3DC/C-CVD did not include much of the converted SiC, as shown in Fig. 14a. This fact implies that the bonding strength between fiber bundles was not sufficiently enhanced. Thus, the fly-out occurred at lower rotation speed than that in the case of pristine Disk Bs because of the mass gain resulting from the Si conversion. On the other hand, 3DC/C-Si sustained a higher rotation speed than that of Disk B by enhancement of inter-bundle bonding strength (Fig. 14b). Estimated bonding toughness in this case was slightly lower than 200 J/m^2. Thus, toughness improvement was about 7-fold. However, the onset speed for fly-out behavior of 3DC/C-Si was still low for used in the turbine disk of the ATREX.

3.6. Machinability of 3DC/C for turbine blades

The sharpness of the turbine blade tip is another key factor in turbo machinery; a sharper edge contributes to higher performance of a turbine system. To avoid problems associated with thermal mismatch stress and/or vibration, it is preferable to form the turbine blades by direct machining of a 3DC/C disk. As a result of the machining, high strength can be expected at the root section of the turbine blades, since fibers in the blade can continue into the disk. However, 3D-C/Cs usually have a coarse bundle texture, so that an extremely sharp edge might exclude reinforcing fiber. Thus, the sharp edge formed by a conventional milling technique easily fractures. Figure 15 shows the edge of the simulated turbine blades with tip radii, R, of 0.1, 0.5, and 1.0 mm. As shown in the figure, the edge could be machined down to $R = 0.5$ mm, and was locally broken at $R = 0.1$ mm. A spin test was conducted on the simulated turbine blade with $R = 0.5$ mm, and it maintained its shape up to 470 m/s without local failure. This speed is high enough for used in the ATREX.

4. CONCLUSIONS

A feasibility study of a carbon-carbon composite turbine disk for used in ATREX was conducted and the following conclusions were drawn.

(1) Fracture speed of 3DC/C was 516 m/s, which speed is high enough for use in ATREX. However, fiber bundle fly-out behavior accompanying the increase in shaft vibration occurred before the total fracture of the disk. The average hoop stress criterion can be adapted to the fracture of the 3DC/C disk used in this study.

(2) The fly-out behavior was characterized as stable/unstable debonding behavior of the fiber bundles from the 3DC/C disk. This behavior was initiated as a result of the sharply terminated edge created by machining of locally curved fiber bundles. A first order approximation based on the simplified fiber-bundle debonding model gave a semi-quantitative understanding of the fly-out behavior. Effective preventive measures against fly-out behavior are the use of finer fiber texture and enhancement of inter-fiber-bundle bonding strength.

(3) Liquid Si impregnation of the surface area of the 3DC/C disk was shown to be effective for preventing fly-out behavior. Although the Si-impregnated 3DC/C in this study exhibited higher resistance to fly-out behavior than did the pristine 3DC/C, the maximum rotation speed was still low for use in ATREX.

(4) Turbine blades made by 3DC/C could be machined by a conventional milling technique with a tip radius = 0.5 mm, and the blade maintained its shape after rotation up to 470 m/s at room temperature.

Acknowledgement

This study was financially supported in part by a grant-in-aid for basic science (Grant No. 11305047) from the Ministry of Education, Science, Sports, Culture and Technology of Japan. The authors would like to thank Mr. Kazunari Shibuya and Yukihiro Takada for their help in the experiments.

REFERENCES

1. T. Sato, N. Tanatsugu, H. Hatta, K. Goto, H. Kobayashi, J. Omi and J. Tomike, in: *10th International Space Planes and Hypersonic Systems and Technologies Conference*, AIAA-2001-1839 (2001).
2. T. Sato, N. Tanatsugu, Y. Naruo, J. Omi, J. Tomike and T. Nishino, *Acta Astronautica* **47** (11), 799–808 (2000).
3. H. Hatta, Y. Kogo, A. Okura, N. Tahatusugu, H. Onabe, T. Mizutani and F. Tomioka, ISAS Report No. 85 (1996) (in Japanese).
4. G. Savage, *Carbon-Carbon Composite*. Chapman and Hall (1993).
5. C. R. Thomas (Ed.), *Essentials of Carbon-Carbon Composite*. Royal Chemical Society, London (1993).
6. J. W. Brockmeyer, Ceramic matrix composite applications in advanced liquid fuel rocket engine turbomachinery, *Trans. ASME, J. Eng. For Gas Turbines and Power* **115**, 58–63 (1993).
7. D. L. Schmidt, K. E. Davidson and L. S. Theibert, Unique applications of carbon-carbon composites, *SAMPE Journal* **35** (3), 27 (1999).
8. A. Ogawa, Y. Sofue, R. Hashimoto, T. Morimoto, F. Zhou and M. Yonaiyama, An application study of C/C composites to turbine disk, Extended Abstract of *The 3rd HYPR International Symposium on Japan National Project* (1999).
9. N. Suzumura, T. Araki, T. Natsumura, S. Masaki, M. Onozuka, H. Onabe, T. Yamamura and K. Yasuhira, Application of ceramic matrix composites to rotating components for advanced gas-generator, in: *Proc. ECCM-8*, Vol. 4, I. Crivelli Visconti (Ed.), pp. 57–64 (1998).
10. Y. Sato and F. Nagai, *Bull. Jap. Soc. Mech. Eng.* **69** (575), 1617–1623 (1966) (in Japanese).
11. Y. Sato, *J. Jap. Soc., Mech. Eng.* **44** (386), 3371–3377 (1978) (in Japanese).
12. T. Hattori, K. Ikegami and H. Shiratori, *J. Japan Soc. Mech. Eng.* **A44**, 845–853 (1978) (in Japanese).
13. Y. Nose, K. Ikegami and H. Shiratori, *J. Japan Soc. Mech. Eng*. **A45**, 81–91 (1978) (in Japanese).
14. A. P. Coppa, in: *Proc. Japan–US CCM-III*, pp. 297–306 (1986).
15. Y. Kogo, H. Hatta, H. Kawada, T. Shigemura, H. Onabe, T. Mizutani and F. Tomioka, Spin burst test of carbon-carbon composites disk, *Compos. Mater.* **32** (11), 1016–1035 (1998).
16. H. Hatta, K. Suzuki, T. Shigei, Y. Sawada and S. Somiya, Strength improvement by densification of C/C composites, *Carbon* **39**, 83–90 (2001).
17. Y. Kogo, H. Hatta, H. Kawada and T. Machida, Effect of stress concentration on the tensile fracture behavior of carbon-carbon composites, *Compos. Mater.* **32** (13), 1273–1294 (1998).
18. H. Hatta, K. Goto, S. Ikegaki, I. Kawahara, M. S. Aly-Hassan and H. Hamada, Tensile strength and fiber/matrix interfacial properties of 2D and 3D-carbon/carbon composites, *J. Euro. Ceram. Soc.* (submitted).
19. H. Hatta, E. Sudo, Y. Kogo and I. Shiota, *J. Japan Inst. Metal.* **62** (9), 861–867 (1998) (in Japanese).
20. W. Krenkel, Fiber ceramics for reentry vehicle hot structures, in: *Proc. 40th Int. Astronautical Congress (IAF)*, pp. 1–7 (1989).

21. J. W. Hutchinson and Z. Suo, Mixed mode cracking in layered materials, *Adv. Appl. Mech.* **29**, 63–191 (1992).
22. H. Tada, P. C. Paris and G. R. Irwin, *Stress Analysis of Cracks Handbook*, 2nd edn. Del Research Corporation (1985).
23. H. Kobayashi, Y. Arai, T. Araki and T. Oku, *J. Soc. Mater. Sci. Jap.* **39**, 1076 (1990) (in Japanese).